



# Relative humidity gradients as a key constraint on terrestrial water and energy fluxes

Yeonuk Kim<sup>1</sup>, Monica Garcia<sup>2</sup>, Laura Morillas<sup>3</sup>, Ulrich Weber<sup>4</sup>, T. Andrew Black<sup>5</sup>, Mark S. Johnson<sup>1,3,6</sup>

<sup>1</sup>Institute for Resources, Environment and Sustainability, University of British Columbia, Vancouver, V6T1Z4, Canada.

<sup>2</sup>Department of Environmental Engineering, Technical University of Denmark, Lyngby, 2800, Denmark.

<sup>3</sup>Center for Sustainable Food Systems, University of British Columbia, Vancouver, V6T1Z4, Canada.

<sup>4</sup>Max Planck Institute for Biogeochemistry, Hans Knoell Strasse 10, 07745 Jena, Germany

<sup>5</sup>Faculty of Land and Food Systems, University of British Columbia, Vancouver, V6T1Z4, Canada.

<sup>6</sup>Department of Earth, Ocean and Atmospheric Sciences, University of British Columbia, Vancouver, V6T1Z4, Canada.

Correspondence to: Yeonuk Kim (yeonuk.kim.may@gmail.com)

**Abstract.** Earth's climate and water cycle are highly dependent on terrestrial evapotranspiration and the associated flux of latent heat. Despite its pivotal role, predictions of terrestrial evapotranspiration remain uncertain due to highly dynamic and spatially heterogeneous land surface dryness. Although it has been hypothesized for over 50 years that land dryness becomes embedded in atmospheric conditions, underlying physical mechanisms for this land-atmospheric coupling remain elusive. Here, we use a novel physically-based evaporation model to demonstrate that near-surface atmospheric relative humidity ( $rh$ ) fundamentally coevolves with  $rh$  at the land surface. The new model expresses the latent heat flux as a combination of thermodynamic processes in the atmospheric surface layer. Our approach is similar to the Penman-Monteith equation but uses only routinely measured abiotic variables, avoiding the need to parameterize surface resistance. We applied our new model to 212 in-situ eddy covariance sites around the globe and to the FLUXCOM global-scale evaporation product. Vertical  $rh$  gradients were widely observed to be near zero on daily to yearly time scales for local as well as global scales, implying an emergent land-atmosphere equilibrium. This equilibrium allows for accurate evaporation estimates using only the atmospheric state and radiative energy, regardless of land surface conditions and vegetation controls. Our results also demonstrate that the latent heat portion of available energy (i.e., evaporative fraction) at local scales is mainly controlled by the vertical  $rh$  gradient. By demonstrating how land surface conditions become encoded in the atmospheric state, this study will improve our fundamental understanding of Earth's climate and the terrestrial water cycle.

## 1 Introduction

Latent heat flux ( $LE$ ) associated with plant transpiration and evaporation from soil and intercepted water (i.e., evapotranspiration, ET) links the water cycle with the terrestrial energy budget. More than half of the incoming radiation energy at the land surface is consumed as  $LE$ , making ET the second largest flux in the terrestrial water balance after



precipitation (Oki and Kanae, 2006). Also,  $LE$  is a controlling factor for near-surface climatic conditions (Ma et al., 2018; Byrne and O’Gorman, 2016). However,  $LE$  predictions remain highly uncertain due to the high spatial and temporal variability in  
 35 land surface dryness, and the difficulty of generalizing the physiological control of ET by stomata. While most research has been devoted to developing and improving rate-limiting parameters constraining  $LE$  (e.g., García et al., 2013; Martens et al., 2017), exploring the governing physics of  $LE$  has received less attention following earlier pioneering work (Penman, 1948; Bouchet, 1963; Monteith, 1965; Priestley and Taylor, 1972).

Climatic conditions over the land surface are getting not only warmer but also drier in recent decades (i.e., decrease  
 40 in relative humidity) (Sherwood and Fu, 2014; Willett et al., 2014; Byrne and O’Gorman, 2018), but land-atmosphere feedback processes shaping the near-surface atmospheric state are still not well understood. In the early 1960’s, Bouchet (1963) hypothesized that land surface dryness is coupled to the atmospheric state through  $LE$ , with the Bouchet hypothesis now widely accepted (Ramírez et al., 2005; Fisher et al., 2008; Mallick et al., 2014). However, the underlying physical mechanisms for this land-atmospheric coupling still remain elusive (McNaughton and Spriggs, 1989). Recently, McColl et al. (2019) introduced a  
 45 novel theoretical perspective on land-atmosphere coupling which is referred to as “Surface Flux Equilibrium (SFE)”. They hypothesized that the surface moistening and heating terms are balanced in the  $rh$  budget of an idealized atmospheric boundary layer at daily to monthly timescale. Under the SFE conditions,  $LE$  can be determined using only the atmospheric state and radiative energy. Although this method performed well compared to actual  $LE$  observations for inland continental sites (McColl and Rigden, 2020), a further investigation is needed to understand how dynamics of turbulent heat fluxes in the  
 50 atmospheric surface layer at sub-daily time scale evolve to the SFE state.

A traditional way to understand the governing physics of the atmospheric surface layer processes is to partition  $LE$  into diabatic and adiabatic processes using the Penman-Monteith (PM) equation (Monteith, 1965), as proposed by Monteith (1981). The PM equation combines the energy balance equation with mass-transfer theory for water vapour and sensible heat, resulting in diabatic (radiative energy-related) and adiabatic (vapour pressure deficit-related) processes for a parcel of air in  
 55 contact with a saturated surface (Monteith, 1981).

$$LE = \underbrace{\frac{S}{S + \gamma \left( \frac{r_a + r_s}{r_a} \right)}}_{\text{Diabatic process}} \cdot Q + \underbrace{\frac{\rho c_p}{S + \gamma \left( \frac{r_a + r_s}{r_a} \right)} \cdot \frac{e^*(T_a) - e_a}{r_a}}_{\text{Adiabatic process}} \quad (1)$$

where  $S$  is the linearized slope of saturation vapour pressure versus temperature ( $\text{hPa K}^{-1}$ ),  $\gamma$  is the psychrometric constant ( $\text{hPa K}^{-1}$ ),  $\rho$  is the air density ( $\text{kg m}^{-3}$ ),  $c_p$  is the specific heat capacity of air at constant pressure ( $\text{MJ kg}^{-1} \text{K}^{-1}$ ), and  $Q$  is available radiative energy (i.e., the difference between net radiation ( $R_n$ ) and soil heat flux ( $G$ ) and expressed in units of  $\text{W m}^{-2}$ ).  $e^*(T_a)$   
 60 is the saturation vapour pressure ( $\text{hPa}$ ) corresponding to the air temperature ( $T_a$ ) measured at a reference height (typically 2 m or eddy flux measurement height), and  $e_a$  is vapour pressure ( $\text{hPa}$ ) at the reference height.  $e^*(T_a) - e_a$  is known as atmospheric vapour pressure deficit (VPD, expressed in units of  $\text{hPa}$ ).  $r_a$  is aerodynamic resistance to heat and water vapour transfer ( $\text{s m}^{-1}$ ), and  $r_s$  is surface resistance to water vapour transfer ( $\text{s m}^{-1}$ ) representing drying soil and/or plant stomatal closure.



In principle, high VPD at the reference height increases the adiabatic term in Eq. (1) (Monteith and Unsworth, 2013).

65 Yet, this “high VPD leads to high  $LE$ ” interpretation cannot be generalized because  $r_s$  increases with VPD due to stomatal closure by vegetation under high VPD conditions (Tan et al., 1978; Novick et al., 2016; Massmann et al., 2019). While the PM equation is useful to explore biological control of  $LE$  through  $r_s$  (Jarvis and McNaughton, 1986), physical mechanisms corresponding to each term in Eq. (1) are less intuitive due to the sensitivity of  $r_s$  to VPD.

Is there a way to mathematically express the physical mechanisms of  $LE$  without requiring  $r_s$ ? Helpfully, Monteith  
 70 (1981) provided another form of the  $LE$  model for the case when the surface does not reach saturation (i.e., the relative humidity ( $rh$ ) of the surface is less than unity), and for which  $r_s$  is not required. Here, we further find that there are two mathematical expressions of  $LE$  which are capable of accounting for the vertical gradients in  $rh$ . The following equations allow us to capture the thermodynamic process governing turbulent heat exchange between the land surface and the atmosphere, including conditions for which the land surface is unsaturated (derivation in Appendix A).

$$75 \quad LE = \underbrace{\frac{rh_s S}{rh_s S + \gamma} \cdot Q}_{\text{Diabatic process: } LE_Q} + \underbrace{\frac{\rho c_p e^*(T_a)}{rh_s S + \gamma} \cdot \frac{rh_s - rh_a}{r_a}}_{\text{Adiabatic process: } LE_G} = LE_Q + LE_G \quad (2)$$

$$LE = \underbrace{\frac{rh_a S}{rh_a S + \gamma} \cdot Q}_{\text{Diabatic process: } LE_{Q'}} + \underbrace{\frac{\rho c_p e^*(T_s)}{rh_a S + \gamma} \cdot \frac{rh_s - rh_a}{r_a}}_{\text{Adiabatic process: } LE_{G'}} = LE_{Q'} + LE_{G'} \quad (3)$$

where  $rh_s$  and  $rh_a$  are  $rh$  at the land surface and the reference height, respectively. Equations (2) and (3) include  $rh_s$  to compensate for eliminating  $r_s$  from the original PM equation. Since the adiabatic process in Eqs. (2) and (3) are controlled by the vertical difference of  $rh$ , we refer to Eqs. (2) and (3) as the proposed  $PM_{rh}$  model (Penman-Monteith equation expressed  
 80 using  $rh$ ) to distinguish it from the original PM model. The two equations represent different thermodynamic paths which will be discussed in the next section. Arguably, applying  $PM_{rh}$  can provide new insights into the fundamental mechanisms of  $LE$ , particularly when it is decomposed into its energy driven diabatic component ( $LE_Q$  or  $LE_{Q'}$ ) and its adiabatic component ( $LE_G$  or  $LE_{G'}$ ) that is driven by the gradient in  $rh$ .

In this paper, we first present the theory of our  $PM_{rh}$  model, and apply it empirically to eddy-covariance observation  
 85 sites. Also, the proportion of net available energy consumed in evapotranspiration, known as the evaporative fraction ( $EF = \frac{LE}{Q}$ ) is decomposed into  $\frac{LE_Q}{Q}$  and  $\frac{LE_G}{Q}$ . Finally, we apply the decomposition approach to a global  $LE$  dataset to understand how  $LE_Q$  and  $LE_G$  vary spatiotemporally in different regions of the world, and discuss how these patterns can help to understand land-atmosphere interactions and potential responses under future climatic conditions.



## 2. Theory

### 90 2.1. Generalized Penman equation

Before discussing  $PM_{th}$  in-depth, we revisit the Penman equation (Penman, 1948) to help with the physical reasoning behind our proposed framework. The widely recognized form of the Penman equation, which was developed as an  $LE$  model for a saturated surface, is as follows:

$$LE = \underbrace{\frac{S}{S+\gamma} \cdot Q}_{\text{Diabatic process}} + \underbrace{\frac{\rho c_p [e^*(T_a) - e_a]}{[S+\gamma] r_a}}_{\text{Adiabatic process}} \quad (4)$$

95 We rearrange this formulation to derive Eq. (5) by factoring out  $e^*(T_a)$  and introducing  $rh_a = \frac{e_a}{e^*(T_a)}$  into the second term.

$$LE = \underbrace{\frac{S}{S+\gamma} \cdot Q}_{\text{Diabatic process}} + \underbrace{\frac{\rho c_p e^*(T_a)}{S+\gamma} \cdot \frac{1-rh_a}{r_a}}_{\text{Adiabatic process}} \quad (5)$$

Equations (4) and (5) are mathematically equivalent, but their interpretations are quite different. In Eq. (4), the adiabatic process is controlled by VPD at the reference height. However, in Eq. (5), the adiabatic process acts over the vertical  $rh$  gradient, i.e. the difference in  $rh$  from the surface ( $rh_s$ ) to the reference height ( $rh_a$ ). Since the Penman equation is a model  
 100 for saturated surfaces,  $1 - rh_a$  in Eq. (5) indicates the difference in  $rh$  over the vertical distance between the ground surface and the reference height. Arguably, Eq. (5) is more thermodynamically sound compared to Eq. (4) since  $rh$  is an ideal-gas approximation to the water activity (Lovell-Smith et al., 2015) which represents the chemical potential of water ( $\mu_w$ ) (Monteith and Unsworth, 2013; Kleidon and Schymanski, 2008). When the vertical gradient of  $rh$  dissipates, the land surface and the atmosphere are in thermodynamic equilibrium (Kleidon et al., 2009). Therefore, taking Eq. (5) instead of Eq. (4) allows us to  
 105 view the adiabatic process of the Penman model as an equilibration process driving land-atmosphere equilibrium by bringing the surface  $\mu_w$  to that of the atmosphere.

As with our interpretation of the Penman model, we can view Eq. (2), as a generalized form of the Penman model. Here, the  $LE_G (= \frac{\rho c_p e^*(T_a)}{rh_s S + \gamma} \frac{rh_s - rh_a}{r_a})$  term of Eq. (2) is an equilibration process between the land and the atmosphere when the land surface is not saturated. It is worth noting that  $LE_G$  can be negative when  $rh_s$  is less than  $rh_a$ . Thus, the  $LE_G$  term acts to  
 110 reduce the vertical  $rh$  gradient. This physical interpretation is consistent with recent findings that the variance of the  $rh$  gradient tends to be minimized over the course of the day, implying that the difference between  $rh_s$  and  $rh_a$  is reduced (Salvucci and Gentine, 2013; Rigden and Salvucci, 2015). The diabatic  $LE_Q (= \frac{rh_s S}{rh_s S + \gamma} Q)$  term can be understood as equilibrium  $LE$  for an unsaturated surface, which we discuss later in section 2.3.

### 2.2. Thermodynamic paths

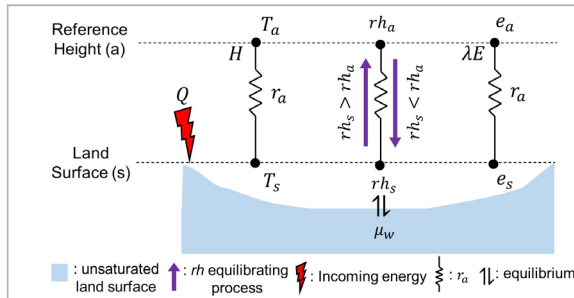
115 How can we interpret the two formulas of  $PM_{th}$  in Eqs. (2) and (3)? To explain the two forms, the psychrometric relationship is applied to a parcel of air near an unsaturated land surface that is under constant pressure and steadily receiving



radiation energy (Monteith, 1981). The initial thermodynamic state of the air parcel can be represented by its temperature and water vapour pressure such as point A in Fig. 1. The initial state is changed by two processes as follows: (1) equilibrating between the land surface ( $rh_s$ ) and the air parcel ( $rh_a$ ), and (2) increasing enthalpy forced by the incoming energy.

120 In the equilibrating process, the air parcel is adiabatically cooled (or heated when  $rh_s < rh_a$ ), while the enthalpy of the parcel is not changed. Therefore, the increase (decrease) in latent heat content in the parcel is exactly balanced by a decrease (increase) in sensible heat ( $A \rightarrow B$  in Fig. 1: trajectory along constant enthalpy line). This process is equivalent to the  $LE_G$  term in Eq. (2). Now, the air parcel is in thermodynamic equilibrium with the land surface (point B in Fig. 1). Then, the air parcel receives energy while the equilibrium is sustained (i.e.,  $rh_s$  is steady), which increases both the temperature and absolute water  
 125 vapour content of the air parcel ( $B \rightarrow C$  in Fig. 1). This process can be expressed as  $LE_Q$  of Eq. (2). Consequently, the thermodynamic state of the air parcel approaches point C in Fig. 1.

However, we should recognize that temperature and vapour pressure are “state” variables meaning that they do not depend on the thermodynamic path by which the system arrived at its final state (Iribarne and Godson, 2012). In the above example, we conceptually followed the adiabatic process first and then the diabatic process (Path 1 in Fig. 1), but one can  
 130 imagine the opposite order. If we choose Path 2 in Fig. 1, the diabatic process comes first, and thus  $rh_a$  instead of  $rh_s$  is preserved while enthalpy increases (i.e.,  $LE_Q'$ ), and the adiabatic process is followed at temperature of  $T_s$  (i.e.,  $LE_G'$ ). Path 2 is described by Eq. (3).

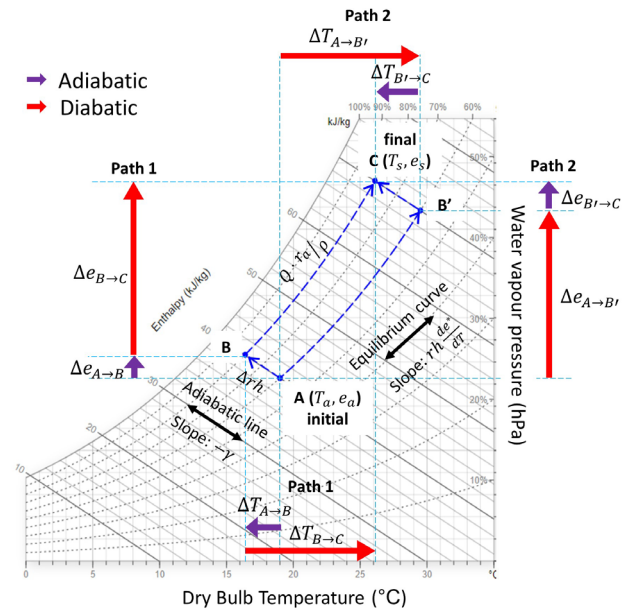


Path 1:

$$\frac{LE \cdot \gamma \cdot r_a}{\rho c_p} = e_s - e_a = \underbrace{\frac{\gamma e^*(T_a)}{rh_s S + \gamma} (rh_s - rh_a)}_{\Delta e_{A \rightarrow B}} + \underbrace{\frac{\gamma rh_s S}{c_p (rh_s S + \gamma)} \frac{Q \cdot r_a}{\rho}}_{\Delta e_{B \rightarrow C}}$$

Path 2:

$$\frac{LE \cdot \gamma \cdot r_a}{\rho c_p} = e_s - e_a = \underbrace{\frac{\gamma rh_a S}{c_p (rh_a S + \gamma)} \frac{Q \cdot r_a}{\rho}}_{\Delta e_{A \rightarrow B'}} + \underbrace{\frac{\gamma e^*(T_s)}{rh_a S + \gamma} (rh_s - rh_a)}_{\Delta e_{B' \rightarrow C}}$$



135 **Figure 1: Schematic conceptualization of the PM<sub>rh</sub> model and psychrometric relationship of PM<sub>rh</sub>. The example psychrometric chart is modified from [drajmarsh.bitbucket.io/psychro-chart2d.html](https://drajmarsh.bitbucket.io/psychro-chart2d.html). Path 1 represents Eq. (2) divided by  $\frac{\rho c_p}{\gamma r_a}$  while Path 2 represents Eq. (3) divided by  $\frac{\rho c_p}{\gamma r_a}$ . Here, the enthalpy change of the air parcel is defined as  $\frac{Q \cdot r_a}{\rho}$  (kJ kg<sup>-1</sup>).**



Therefore, one can interpret the two forms of  $PM_{rh}$  in Eqs. (2) and (3) as two thermodynamic paths where the diabatic and adiabatic processes occur simultaneously. It should be noted that the diabatic and adiabatic processes in  $PM_{rh}$  are “path” functions and thus they vary by path. For instance,  $LE_Q$  is slightly higher than  $LE_Q'$  when  $rh_s > rh_a$ .

### 2.3. Equilibrium $LE$ for an unsaturated surface

Another distinct characteristic of the  $PM_{rh}$  model is the way it defines equilibrium at the land-atmosphere interface. Unlike many previous studies which focused on the VPD budget (McNaughton and Jarvis, 1983; Priestley and Taylor, 1972; Raupach, 2001), land-atmosphere equilibrium is achieved in the  $PM_{rh}$  model when the vertical  $rh$  gradient (i.e., the  $\mu_w$  gradient) dissipates. That is, if  $rh_s \approx rh_a$ , then it follows that  $LE_G$  (or  $LE_G'$ ) is zero and thus  $LE$  becomes

$$LE \approx \frac{rh_a S}{rh_a S + \gamma} Q \quad (6)$$

We note that Equation (6) is identical to the SFE theory recently introduced by McColl et al. (2019). They hypothesized that in many continental regions, the near surface atmosphere is in state of equilibrium, where the surface moistening and surface heating terms are balanced in the  $rh$  budget, especially at longer time scales. Equation (6) successfully predicted observed  $LE$  at daily and multiday time scales for inland regions (McColl and Rigden, 2020), which implies the vertical  $rh$  gradient tends to zero. This is logical in that  $LE_G$  itself operates to diminish the vertical  $rh$  gradient.

When both land surface and atmosphere are saturated (i.e.,  $rh_s \approx rh_a \approx 1$ ), equation (6) becomes classical equilibrium  $LE$  (i.e.,  $LE \approx \frac{S}{S+\gamma} Q$ ). This is consistent with a classical definition of equilibrium  $LE$  that defines equilibrium  $LE$  as evaporation from a saturated surface into saturated air (Eichinger et al., 1996; Raupach, 2001; McColl, 2020). Therefore, we can regard Eq. (6) as a generalized equilibrium  $LE$  for an unsaturated surface.

## 3. Materials and Methods

In the following sections, we present a novel physical decomposition of  $LE$  from  $PM_{rh}$  into  $LE_Q$  and  $LE_G$  components to aid in understanding the governing physics of  $LE$ . We conducted a detailed diagnostic analysis of the  $PM_{rh}$  model using the multi-year record of an eddy covariance (EC) flux observation site located in a wet-dry tropical climate. We also applied the  $PM_{rh}$  model to the 212 EC sites represented in the FLUXNET2015 dataset (Pastorello et al., 2020), and to the FLUXCOM global  $LE$  product (Jung et al., 2019). We describe the local and global datasets and analysis methods here before presenting the results.

### 3.1. In-situ EC flux observation

In-situ half-hourly EC observations used in this study were made from 2015 to 2018 on a ratoon sugarcane farm in the province of Guanacaste, Costa Rica (10°25'07.60"N; 85°28'22.22"W). The site has a wet-dry tropical climate with a dry season from December to March and a median monthly air temperature ranging from 27 °C to 30 °C. The study site experienced a





significant drought in 2015 (Hund et al., 2018; Morillas et al., 2019). The site was irrigated occasionally during dry seasons via furrow irrigation events, except for 2016 when there was no irrigation due to crop replanting. Due to the ratooning practice (i.e., sugarcane cutting each year followed by resprouting without replanting, detailed explanation in the Supplement), the sugarcane growing seasons varied by year, which provided an opportunity to explore distinct and varied combinations of land surface vs. atmospheric aridity conditions.

The measured  $LE$  and sensible heat flux ( $H$ ) were quality controlled following Morillas et al. (2019) (details in the Supplement). For the study period, the surface energy balance closure (i.e.,  $\frac{LE+H}{R_n-G}$ ) of 30 min data was 86 %, which is typical of high-quality eddy-covariance data sets (Wilson et al., 2002). When canopy height was less than 1 m, the surface energy balance was almost closed (97%), whereas the closure was 83 % when canopy height was higher than 1 m. Considering a possible significant role of unmeasured canopy and soil heat storages (Leuning et al., 2012; Eshonkulov et al., 2019) and the homogenous landscape of the study site (Foken, 2008; Stoy et al., 2013), we did not force the energy closure. Therefore, we defined  $Q$  as the sum of  $LE$  and  $H$  instead of  $R_n - G$ . In doing so, we in effect attribute the cause of the surface energy imbalance to unmeasured heat storage terms following Moon et al. (2020).

In order to decompose  $LE$  into  $LE_Q$  and  $LE_G$ , we first estimated half-hourly aerodynamic resistance ( $r_a$ ) by considering aerodynamic resistance to momentum transfer and the additional boundary layer resistance for heat and mass transfer (or excess resistance) (Thom, 1972; Knauer et al., 2018).

$$r_a = \frac{\ln\left[\frac{z_r-d}{z_{0m}}\right] - \psi_h}{ku_*} + 6.2u_*^{-0.67} \quad (7)$$

The first term on the right-hand side of Eq. (7) is the aerodynamic component and the second term is the boundary layer component. Here,  $u_*$  is friction velocity,  $k$  is the von Kármán constant (0.41),  $d$  is the zero-plane displacement height ( $d = 0.7z_h$ ),  $z_{0m}$  is the roughness length for momentum ( $z_{0m} = 0.1z_h$ ),  $\psi_h$  is the integrated form of the stability correction function.  $z_h$  is canopy height based on manual measurements taken during regular maintenance visits.  $r_a$  was estimated using bigleaf R package (Knauer et al., 2018).

By rearranging Eq. (2),  $rh_s$  can be calculated using

$$rh_s = \frac{\gamma LE r_a / \rho c_p + e_a}{SH r_a / \rho c_p + e^*(T_a)} \quad (8)$$

Negative  $H$  and inaccurate  $r_a$  modelling sometimes yielded negative  $rh_s$  or values greater than one, especially at nighttime. In these cases,  $rh_s$  was assigned the value of one following the approach described in the bigleaf R package (Knauer et al., 2018). We then estimated  $LE_Q$  and  $LE_G$  from Eq. (2).

In order to explore the time scale of the covariances for  $LE \sim LE_Q$  and  $LE \sim LE_G$  in the frequency domain, we applied wavelet coherence analysis using WaveletComp R package (Roesch and Schmidbauer, 2014). The package is designed to apply the continuous wavelet transform using Morlet wavelet, which is a popular approach to analyze hydrological and micrometeorological datasets (Hatala et al., 2012; Johnson et al., 2013). A total time series of half-hourly decomposed  $LE$  for the 4-year measurement period was used to estimate localized coherence and phase angle. The wavelet coherence can be



interpreted as the local correlation between two variables in the frequency-time domain (where red indicates high correlation).  
 A 0° phase angle (arrow pointing right) indicates periods of positive correlation while a 180° phase angle (arrow pointing left)  
 indicates periods of negative correlation.

### 3.2. FLUXNET2015

The daily scale FLUXNET2015 dataset, which includes 212 empirical eddy-covariance flux tower sites around globe  
 (Pastorello et al., 2020), was used in this study. The turbulent heat fluxes, net radiation, soil heat flux, air temperature, relative  
 humidity, wind speed, friction velocity, and barometric pressure were obtained from the dataset. For this analysis, we only  
 included daily data for periods for which the quality control flag indicated more than 80 % half-hourly data were present (i.e.,  
 measured data in general, or good quality gap-filled data in cases of partially missing data).

In order to decompose daily  $LE$  into  $LE_Q$  and  $LE_G$ , we estimated daily aerodynamic resistance ( $r_a$ ) by Eq. (9) instead  
 of Eq. (7) since canopy and measurement heights are unknown (Thom, 1972; Knauer et al., 2018).

$$r_a = \frac{u_*^2}{u(z_r)} + 6.2u_*^{-0.67} \quad (9)$$

where,  $u(z_r)$  is reference height wind speed.  $r_a$  was estimated using the bigleaf R package (Knauer et al., 2018) and  $rh_s$  was  
 calculated from Eq. (8).

$LE_Q$  and  $LE_Q'$  were calculated using  $rh_a$  and  $rh_s$  following Eqs. (2) and (3), and then  $LE_G$  and  $LE_G'$  were calculated  
 by subtracting  $LE_Q$  and  $LE_Q'$  from  $LE$ . To calculate  $LE_Q$  and  $LE_Q'$ , we define  $Q$  as  $LE + H$ , but it should be noted that this  
 approach can include systematic uncertainty since the sum of  $LE$  and  $H$  measured by eddy covariance is typically lower than  
 $R_n - G$  (i.e., conditions referred to as the energy balance closure problem (Wilson et al., 2002)). To investigate the effect of a  
 lack of energy balance closure on resulting  $LE$  terms, we provide Fig. S1 that was generated by 1) defining  $Q$  as  $R_n - G$ , and  
 2) correcting  $LE$  and  $H$  based on the assumption that the Bowen ratio ( $B = H/LE$ ) is correct (Pastorello et al., 2020).

### 3.3. FLUXCOM

The FLUXCOM dataset (Jung et al., 2019) is a global-scale machine learning ensemble product which upscales FLUXNET  
 observations (Baldocchi et al., 2001) using Moderate Resolution Imaging Spectroradiometer (MODIS) satellite data and  
 reanalysis meteorological data. In this study we used the monthly  $LE$  FLUXCOM dataset (0.5° resolution) modelled using  
 MODIS and ECMWF ERA5 reanalysis data (Hersbach et al., 2020).

We obtained  $Q$  and  $LE$  from the FLUXCOM output, and air temperature and dewpoint temperature were retrieved  
 from ERA5 monthly averaged data (2 m height).  $rh$ ,  $S$ , and  $\gamma$  were calculated from ERA5 data, and then  $LE_Q'$  was calculated.  
 $LE_G'$  was then estimated by subtracting  $LE_Q'$  from  $LE$ .





## 4. Results

### 4.1. Decomposition analysis of in-situ EC flux observation

Application results of the  $PM_{rh}$  model to the observed  $LE$  at an irrigated sugarcane farm in Costa Rica are depicted in Fig. 2. The decomposition analysis of observed  $LE$  shows that while  $LE_Q$  is the major component of  $LE$ ,  $LE_G$  variability plays a non-negligible role in seasonal and interannual behaviour of  $LE$ . In terms of absolute magnitude,  $LE_Q$  term can closely approximate  $LE$ , and  $LE_G$  only represents 15% of total evaporation. Also, positive coherence between  $LE$  and  $LE_Q$  was strong over the entire period of observation, particularly at diurnal to multiday time scales (0.5~32 days), implying variability of  $LE$  is largely determined by  $LE_Q$  variability (i.e., red colored regions in Fig. 2 (c)).

Nevertheless,  $LE$  and  $LE_G$  also had a strong positive correlation in longer time scales (32~365 days) (i.e., red colored regions in Fig. 2 (d)). When the land surface is dry after harvests or no dry season irrigation, a negative correlation between  $LE$  and  $LE_G$  at diurnal time scale was observed. Also, we found that EF variability is mostly determined by  $LE_G$  variability since the diurnal and seasonal signal of  $Q$  is removed from  $LE$  in EF. Interestingly, the annual mean  $LE_G$  was the highest in 2015, a drought year in which  $rh_a$  was generally lower than for the other years, while the annual mean  $LE_G$  was close to zero in 2016 when there was no application of dry season irrigation due to crop replanting.

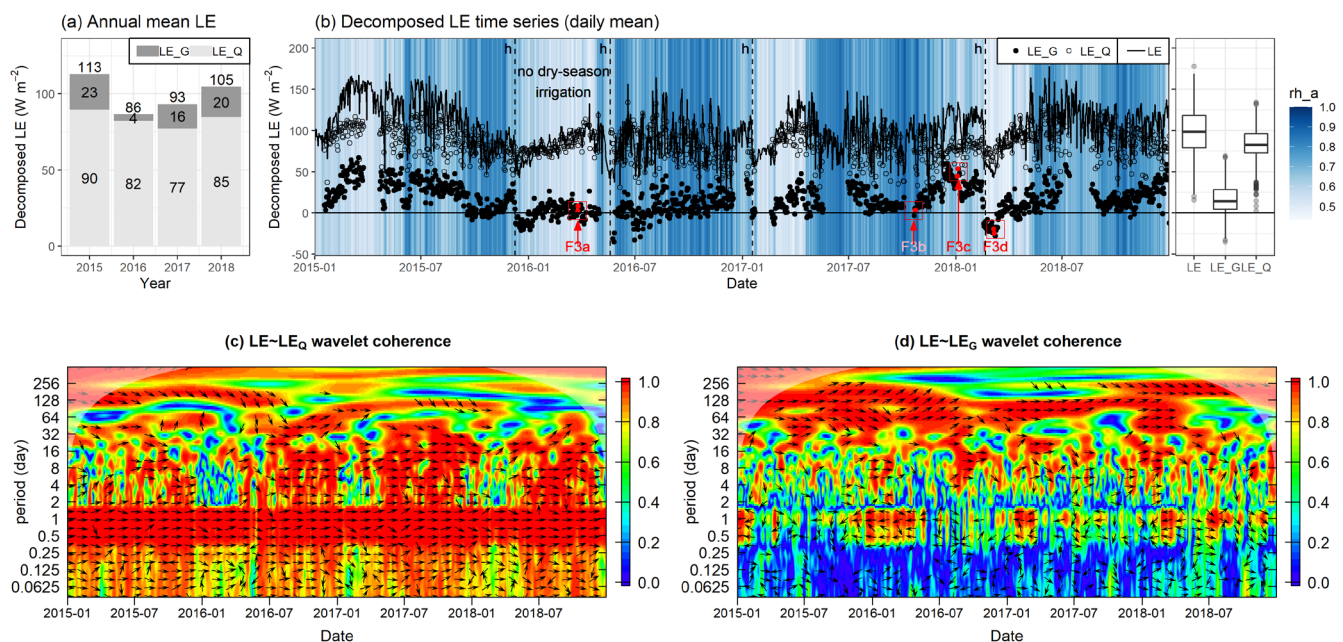


**Figure 2:** Time series of  $LE$ ,  $LE_Q$ , and  $LE_G$  for the sugarcane EC tower site in Costa Rica. Panel (a) is mean annual  $LE$  and its components and (b) is a time series of daily mean values with a background color of  $rh_a$ . Dashed lines with “h” in panel (b) indicate sugarcane harvest. Panels (c) and (d) are wavelet coherence of  $LE$  with  $LE_Q$  and  $LE$  with  $LE_G$ . Red and blue colors indicate high and low correlation, respectively. Arrows (pointing right: in-phase; left: antiphase) only appear when the coherence is significant ( $p < 0.01$ ).



To explore the diurnal behaviour of decomposed  $LE$ , we selected different surficial and atmospheric conditions when  $LE_G$  was zero, positive, or negative in Fig. 3. In the 2016 dry season,  $LE_G$  was close to zero as a daily average value, as a result of negative daytime and positive nighttime  $LE_G$  values due to dry air and dry soil conditions (no irrigation) and an undeveloped vegetation canopy (Fig. 3 (a)). Daily  $LE_G$  was also close to zero during wet season conditions (e.g., Fig. 3 (b)). In this case,  $LE_G$  was near zero during both daytime and nighttime periods due to near saturated atmospheric and land surface conditions. These two cases show that “dry land-dry air” or “wet land-wet air” conditions can each lead to daily scale land-atmosphere equilibrium, although the diurnal pattern of  $LE_G$  is starkly different for dry land-dry air vs. wet land-wet air conditions.

Meanwhile, when  $rh_a$  was low and the canopy was well-developed,  $LE_G$  was found to be positive during both daytime and nighttime periods (Fig. 3 (c)). On the other hand, during post-harvest conditions when vegetative canopy cover was minimal and air and soil moisture levels were low, daily  $LE_G$  was found to be negative as a result of negative daytime and positive nighttime  $LE_G$  (Fig. 3 (d)). Regarding the overall diurnal pattern,  $LE_G$  generally declined during the morning and increased in the afternoon, which is consistent with the well-known diurnal pattern of EF (Gentine et al., 2011; Gentine et al., 2007) (Fig. 3 (e)).

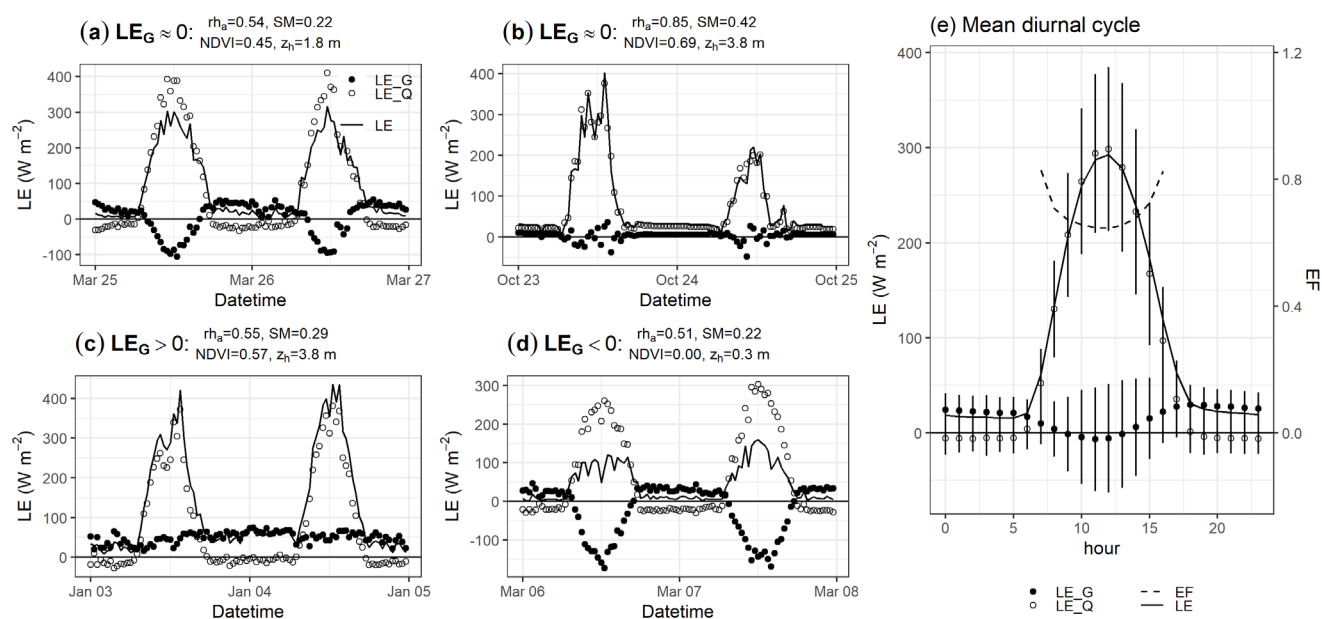


**Figure 3: Half-hourly time series indicated in Figure 2 (b). Here,  $rh_a$  is mean atmospheric relative humidity,  $SM$  is volumetric soil water content,  $NDVI$  is normalized difference vegetation index, and  $z_h$  is canopy height. Panel (e) presents the long-term mean diurnal cycle of decomposed  $LE$  (dots) and  $EF$  (dashed line).**



## 4.2. Decomposition analysis of FLUXNET2015 dataset

One of the interesting findings from the decomposition analysis of FLUXNET2015 dataset was that differences between  $LE_Q$  (Eq. (2)) and  $LE_Q'$  (Eq. (3)), as well as differences between  $LE_G$  and  $LE_G'$ , are marginal at a daily time scale (Fig. 4 (a1) and (a2)). This result implies that although the diabatic and adiabatic processes expressed by Eqs. (2) and (3) are different in magnitude (see section 2.2), their difference is practically negligible. This is an important point since  $LE_Q'$  can be determined simply and directly using by reference height meteorological measurements, while  $LE_Q$  is required to know  $rh_s$ .

Another important finding of the decomposition analysis is the global-scale land-atmosphere equilibrium. Our analysis in Fig. 4 indicates that the mean value of daily  $LE_G$  of all FLUXNET2015 sites is close to zero, implying the global mean  $rh$  gradient is near zero at a daily time scale. Importantly,  $LE$  is primarily determined by  $LE_Q$  ( $R^2 = 0.65$ ) instead of  $LE_G$  ( $R^2 = 0.18$ ). Nevertheless, FLUXNET2015 data also suggests that  $LE_G$  is the main driver of local-scale variability of EF at the daily time scale (Fig. 4 (c1) and (c2)). It should be noted that Fig. 4 and Fig. S1 (energy balance corrected version) are almost identical, implying that the lack of surface energy balance closure for EC observations does not significantly impact our analyses and interpretations.

## 4.3. Decomposition analysis of FLUXCOM dataset

We then applied the  $PM_{rh}$  model to the FLUXCOM dataset, a benchmark global  $LE$  data product (Jung et al., 2019). As shown in Fig. 5 (a) and (c), the spatial patterns of the annual mean  $LE$  and  $LE_Q'$  were similar. The monthly time series of global  $LE$  and its two components in Fig. 5 (e1) show that  $LE_G'$  is consistently close to zero and that spatial variability of  $LE$  is mostly determined by  $LE_Q'$  ( $R^2 = 0.85$ ) rather than by  $LE_G'$  ( $R^2 = 0.18$ ) (Fig 5. (f1) and (f2)). This result is consistent with Eq. (6) and the SFE theory. In other words, the land surface is generally under thermodynamic equilibrium with the atmosphere at the global-annual scale (i.e.,  $rh_s \approx rh_a$ ).

However, while mean annual  $LE_G'$  was close to zero in broad areas (particularly in high latitude regions), it was distinctly positive or negative at the annual scale for many regions (Fig. 5 (d)). In humid tropical regions like the Amazon basin where moisture convergence is large,  $LE_G'$  was generally positive, whereas arid regions such as Australia were characterized by negative  $LE_G'$  (Fig. 5 (e3) and (e4)). Here, positive  $LE_G'$  (i.e.,  $rh_s > rh_a$ ) indicates the land surface is wetter than the near-surface atmosphere while negative  $LE_G'$  (i.e.,  $rh_s < rh_a$ ) implies a drier land surface than the atmosphere. The spatial pattern of  $LE_G'$  is similar to the spatial pattern of EF (Fig. 5 (b)). The finding that that the spatial variation of EF is primarily controlled by  $LE_G'$  instead of  $LE_Q'$  was supported by correlation analyses ( $R^2 = 0.60$  for  $EF \sim LE_G'$  and  $R^2 = 0.28$  for  $EF \sim LE_Q'$ ; Fig. 5 (f3) and (f4)).

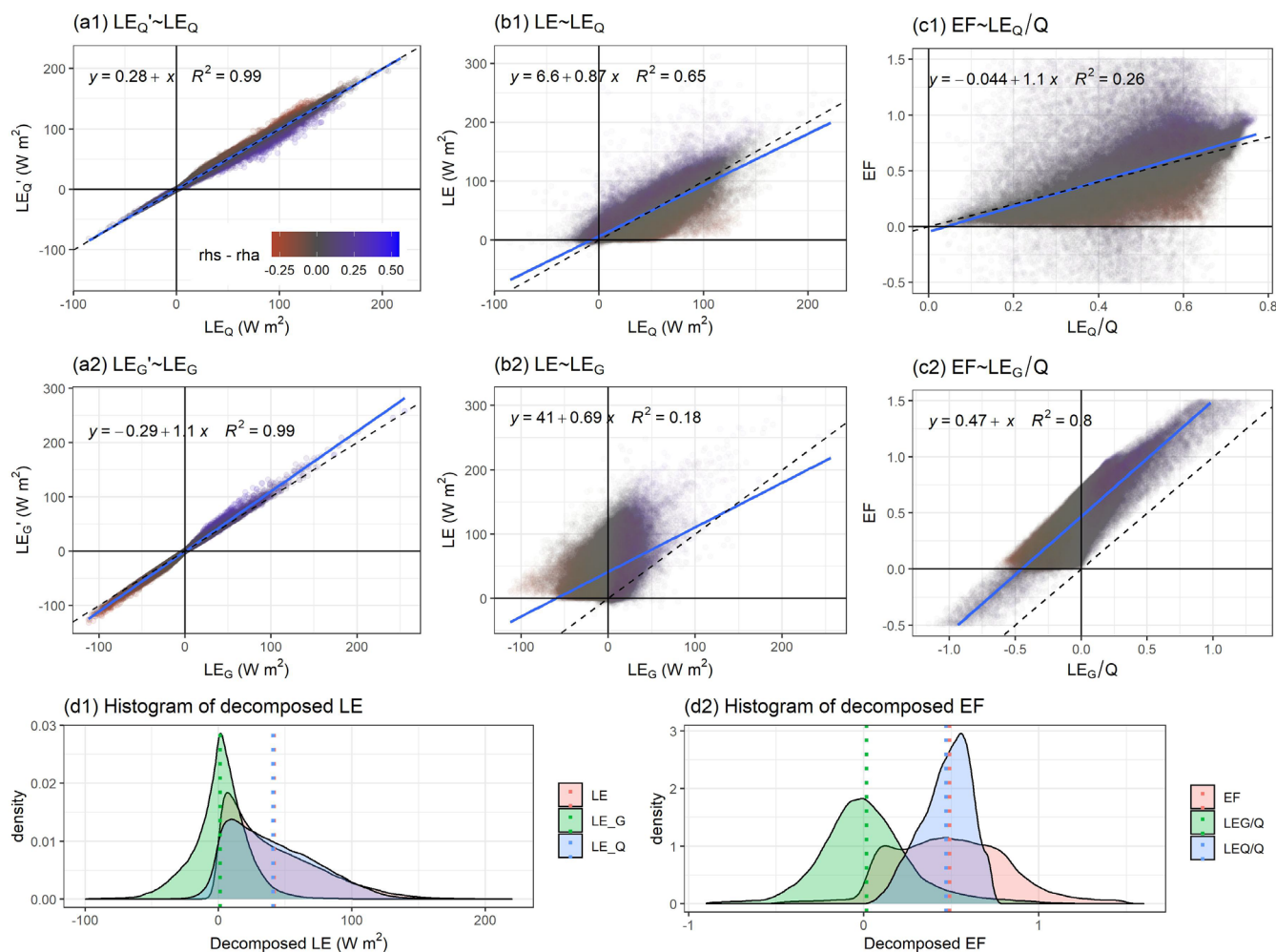


**Figure 4:** FLUXNET2015 daily scale decomposed  $LE$  for 212 sites and 1532 site-years. Panels (a1) and (a2) are linear regressions of  $LE_Q'$  on  $LE_Q$  and  $LE_G'$  on  $LE_G$ . Panels (b1) and (b2) are linear regressions of  $LE$  on  $LE_Q$  and  $LE$  on  $LE_G$ . Panels (c1) and (c2) are linear regressions of  $EF$  on  $LE_Q/Q$  and  $EF$  on  $LE_G/Q$ . In these panels, daily  $EF$  data within a range from -1 to 1.5 are only shown. Here, dashed lines are one-to-one lines, blue lines are regression lines, and color represents  $rhs - rha$ . Panel (d1) and (d2) are histograms of decomposed  $LE$  and  $EF$  with mean values (dotted lines). To correct for lack of energy balance closure,  $Q$  was set equal to  $LE + H$  in all calculations.

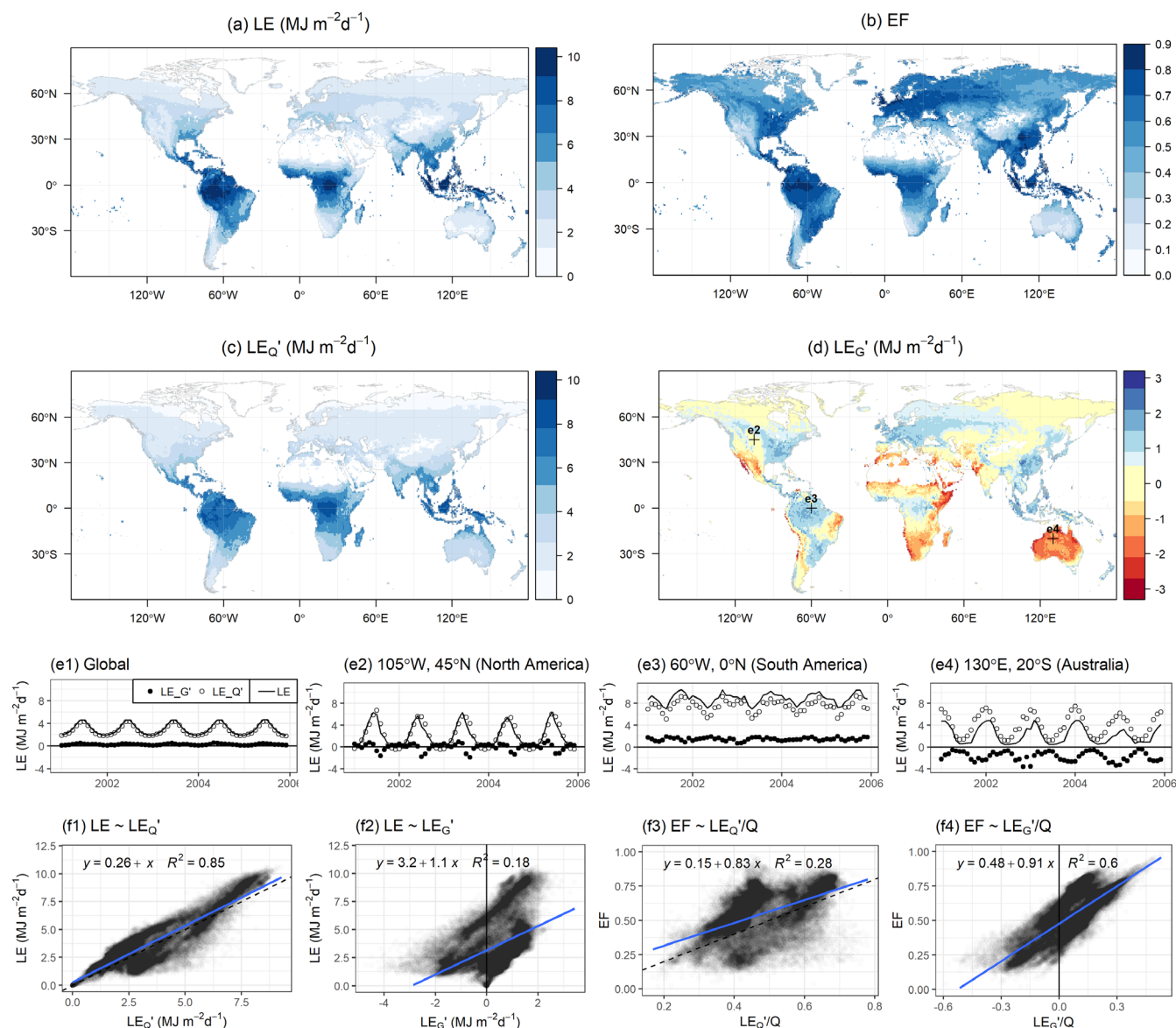


**Figure 5:** Mean annual  $LE$ ,  $EF$ ,  $LE_Q'$ , and  $LE_G'$  from 2001 to 2005 (panels (a), (b), (c), and (d), respectively). Panel (e1) is a time series of monthly global average  $LE$  and the two components,  $LE_G'$  and  $LE_Q'$ . Panels (e2), (e3), and (e4) are time series at specific locations highlighted in panel (d). Panels (f1), (f2), (f3), and (f4) are spatial linear regressions of  $LE$  on  $LE_Q'$ ,  $LE$  on  $LE_G'$ ,  $EF$  on  $LE_Q'/Q$ , and  $EF$  on  $LE_G'/Q$ , respectively.





## 5. Discussion

Salvucci and Gentile (2013) found that the variance of the  $rh$  gradient tends to be minimized over the course of the day. Based on this empirical finding, they developed an approach to predict  $LE$  only using standard meteorological measurements, and this approach accurately predicted actual  $LE$  (Rigden and Salvucci, 2015, 2017). Our  $PM_{rh}$  model provides theoretical support for their approach in that  $LE_G$  acts to reduce the  $rh$  gradient. Indeed, the U-shape diurnal cycles of  $LE_G$  in Fig. 3 (positive nighttime and negative daytime) show the direction and the magnitude of the equilibration process of  $rh$  gradient at a sub-daily scale resulting in a small gradient of  $rh$  on daily average.

Over the course of the day,  $rh_a$  coevolves with  $rh_s$  through the equilibration process, and thus the land surface moisture status is linked to  $rh_a$ . This interpretation is also related to the Bouchet's complementary hypothesis (Bouchet, 1963). Bouchet hypothesized that land surface wetness is coupled to the atmospheric state when there is negligible advection of humid air entering the system. In our  $PM_{rh}$  model,  $rh_s$  and  $rh_a$  are coevolving and consequently, they can be equal at daily time scale both "dry land-dry air" and "wet land-wet air" conditions (Fig. 3). This shows how land surface conditions become embedded in the near-surface atmospheric state.

As described in the theory section, land-atmosphere equilibrium is achieved when  $LE_G$  approaches zero and thus  $LE$  reduces to Eq. (6). The decomposed terms derived from both the empirical FLUXNET2015 and model-based FLUXCOM datasets show that the global mean for  $LE_G$  is near zero, implying global-scale land-atmosphere equilibrium (Fig. 4 and Fig. 5). This result extends the SFE theory of McColl et al. (2019). Although,  $LE_G$  is not always near zero (e.g., in low latitude regions where the influence of the ocean and atmospheric circulation on  $rh_a$  is significant (Byrne and O'Gorman, 2018)), moisture convergence and divergence at the global-scale tend to balance each other out, resulting in global-scale land-atmosphere equilibrium.

A number of important implications emerge from the global scale land-atmosphere equilibrium. (i)  $rh_a$  is a close approximation of  $rh_s$  at the global scale, and thus the decreasing trend of  $rh_a$  over the land surface predicted by climate models (Byrne and O'Gorman, 2016) and empirically observed (Willett et al., 2014) may indicate not only drier climatic conditions but also drier conditions for the land surface and soil moisture. (ii) Equation (6), which can be readily determined using standard meteorological measurements, can provide a fundamental benchmark of global scale  $LE$  which can be used to evaluate sophisticated land surface models.

## 6. Conclusions

We have shown that our novel  $PM_{rh}$  model provides a new opportunity to understand the governing physics of the terrestrial energy budget. Specifically, the  $PM_{rh}$  model helps to illustrate how the land surface conditions become encoded to the atmospheric state. "Dry land-dry air" or "wet land-wet air" conditions can each lead to daily scale land-atmosphere equilibrium. Our findings suggest that while  $LE_G$  is a primary component determining EF, spatiotemporal variability of  $LE_Q$  alone can adequately represent the variability of  $LE$ . We found global-scale land-atmosphere equilibrium at daily to annual scales, which



implies that  $LE$  can be simply determined by the atmospheric state and radiative energy without any surface constraint required to represent spatial heterogeneity and physiological influences. Therefore, our model can provide a fundamental benchmark against which  $LE$  predictions derived from climate models can be assessed. Questions remain regarding how  $LE_Q$  and  $LE_G$  will be influenced in relation to changing climatic and land surface conditions, and how these changes might affect the climate system at differing spatial and temporal scales through positive or negative feedbacks.

## Appendix A

<p><b>Derivation of Equation (2)</b>  <math>LE</math> and <math>H</math> can be written using aerodynamic resistance for water vapour (<math>r_{av}</math>) and sensible heat (<math>r_{aH}</math>) as follows</p> $LE = \frac{\rho c_p r h_s e^*(T_s) - r h_a e^*(T_a)}{\gamma r_{av}} \quad (A1)$ $H = \rho c_p \frac{T_s - T_a}{r_{aH}} \quad (A2)$ <p>To express <math>LE</math> as a function of <math>T_a</math> and <math>r h_s</math>, adding <math>-r h_s e^*(T_a) + r h_s e^*(T_a)</math> to the numerator of (A1) yields:</p> $LE = \frac{\rho c_p r h_s e^*(T_s) - r h_s e^*(T_a) + r h_s e^*(T_a) - r h_a e^*(T_a)}{\gamma r_{av}} = \frac{\rho c_p r h_s \frac{e^*(T_s) - e^*(T_a)}{r_{av}} + \rho c_p e^*(T_a) \frac{r h_s - r h_a}{r_{av}}}{\gamma} \quad (A3)$ <p>Next, we use the linearized slope of <math>e^*</math> (<math>\frac{e^*(T_s) - e^*(T_a)}{T_s - T_a} \approx \frac{de^*}{dT}  _{T=T_a} = S</math>) to give</p> $LE = \frac{\rho c_p r h_s S}{\gamma} \frac{T_s - T_a}{r_{av}} + \frac{\rho c_p}{\gamma} e^*(T_a) \frac{r h_s - r h_a}{r_{av}} \quad (A4)$ <p>If we assume <math>r_{aH} \approx r_{av} \approx r_a</math>, Eq. (A4) becomes</p> $LE = r h_s \frac{S}{\gamma} H + \frac{\rho c_p}{\gamma} e^*(T_a) \frac{r h_s - r h_a}{r_a} \quad (A5)$ <p>Then, substituting the surface energy balance (<math>H = Q - LE</math>) into the first term of Eq. (A5):</p> $LE = \underbrace{\frac{r h_s S}{r h_s S + \gamma} Q}_{Diabatic} + \underbrace{\frac{\rho c_p e^*(T_a)}{r h_s S + \gamma} \frac{r h_s - r h_a}{r_a}}_{Adiabatic} \quad (A6)$	<p><b>Derivation of Equation (3)</b>  <math>LE</math> and <math>H</math> can be written using aerodynamic resistance for water vapour (<math>r_{av}</math>) and sensible heat (<math>r_{aH}</math>) as follows</p> $LE = \frac{\rho c_p r h_s e^*(T_s) - r h_a e^*(T_a)}{\gamma r_{av}} \quad (A7)$ $H = \rho c_p \frac{T_s - T_a}{r_{aH}} \quad (A8)$ <p>To express <math>LE</math> as a function of <math>T_s</math> and <math>r h_a</math>, adding <math>-r h_a e^*(T_s) + r h_a e^*(T_s)</math> to the numerator of (A7) yields:</p> $LE = \frac{\rho c_p r h_s e^*(T_s) - r h_a e^*(T_s) + r h_a e^*(T_s) - r h_a e^*(T_a)}{\gamma r_{av}} = \frac{\rho c_p e^*(T_s) \frac{r h_s - r h_a}{r_{av}} + \rho c_p r h_a \frac{e^*(T_s) - e^*(T_a)}{r_{av}}}{\gamma} \quad (A9)$ <p>Next, we use the linearized slope of <math>e^*</math> (<math>\frac{e^*(T_s) - e^*(T_a)}{T_s - T_a} \approx \frac{de^*}{dT}  _{T=T_a} = S</math>) to give</p> $LE = \frac{\rho c_p}{\gamma} e^*(T_s) \frac{r h_s - r h_a}{r_{av}} + \frac{\rho c_p r h_a S}{\gamma} \frac{T_s - T_a}{r_{av}} \quad (A10)$ <p>If we assume <math>r_{aH} \approx r_{av} \approx r_a</math>, Eq. (A10) becomes</p> $LE = \frac{\rho c_p}{\gamma} e^*(T_s) \frac{r h_s - r h_a}{r_a} + r h_a \frac{S}{\gamma} H \quad (A11)$ <p>Then, substituting the surface energy balance (<math>H = Q - LE</math>) into the second term of Eq. (A11):</p> $LE = \underbrace{\frac{\rho c_p e^*(T_s)}{r h_a S + \gamma} \frac{r h_s - r h_a}{r_a}}_{Adiabatic} + \underbrace{\frac{r h_a S}{r h_a S + \gamma} Q}_{Diabatic} \quad (A12)$
--	--





*Data availability.* The FLUXNET2015 dataset is available in <https://fluxnet.org/data/fluxnet2015-dataset/>. The highlighted  
 350 sugarcane eddy covariance site dataset will be available in AmeriFlux (<https://ameriflux.lbl.gov/>). The FLUXCOM dataset is  
 available in <http://www.fluxcom.org/>.

*Author contribution.* Y.K. and M.S.J. designed research; U.W. provided FLUXCOM data; Y.K., L.M., and M.S.J. performed  
 research; Y.K. analyzed data; Y.K., M.G., T.A.B, L.M., and M.S.J. wrote the paper.

355

*Competing interests.* The authors declare no conflict of interest.

*Acknowledgements.* We want to thank Dr. Iain Hawthorne, Pável Bautista, Dr. Silja Hund, Cameron Webster, Gretel  
 Rojas Hernandez, Guillermo Duran Sanabria, Dr. Andrea Suarez Serrano, Dr. Ana Maria Duran, Martin Martinez, and Dr.  
 360 Fermín Subirós Ruiz for field and logistical support. We also thank Dr. Martin Jung, the principal investigator of the  
 FLUXCOM dataset. The authors would like to thank the EU and NSERC for funding, in the frame of the collaborative  
 international Consortium AgWIT financed under the ERA-NET WaterWorks2015 Cofunded Call. This ERA-NET is an  
 integral part of the 2016 Joint Activities developed by the Water Challenges for a Changing World Joint Programme Initiative  
 (Water JPI).

## 365 References

- Baldocchi, D., Falge, E., Gu, L., Olson, R., Hollinger, D., Running, S., Anthoni, P., Bernhofer, C., Davis, K., and Evans, R.: FLUXNET: A  
 new tool to study the temporal and spatial variability of ecosystem-scale carbon dioxide, water vapor, and energy flux densities,  
 Bulletin of the American Meteorological Society, 82, 2415-2434, 10.1175/1520-0477(2001)082<2415:FANTTS>2.3.CO;2 2001.
- Bouchet, R. J.: Evapotranspiration réelle et potentielle, signification climatique, IAHS Publ, 62, 134-142, 1963.
- 370 Byrne, M. P., and O’Gorman, P. A.: Understanding Decreases in Land Relative Humidity with Global Warming: Conceptual Model and  
 GCM Simulations, Journal of Climate, 29, 9045-9061, 10.1175/jcli-d-16-0351.1, 2016.
- Byrne, M. P., and O’Gorman, P. A.: Trends in continental temperature and humidity directly linked to ocean warming, Proceedings of the  
 National Academy of Sciences, 115, 4863-4868, 10.1073/pnas.1722312115, 2018.
- 375 Eichinger, W. E., Parlange, M. B., and Stricker, H.: On the Concept of Equilibrium Evaporation and the Value of the Priestley-Taylor  
 Coefficient, Water Resources Research, 32, 161-164, 10.1029/95wr02920, 1996.
- Eshonkulov, R., Poyda, A., Ingwersen, J., Pulatov, A., and Streck, T.: Improving the energy balance closure over a winter wheat field by  
 accounting for minor storage terms, Agricultural and Forest Meteorology, 264, 283-296, 10.1016/j.agrformet.2018.10.012, 2019.
- Fisher, J. B., Tu, K. P., and Baldocchi, D. D.: Global estimates of the land-atmosphere water flux based on monthly AVHRR and ISLSCP-  
 II data, validated at 16 FLUXNET sites, Remote Sensing of Environment, 112, 901-919, 10.1016/j.rse.2007.06.025, 2008.
- 380 Foken, T.: The energy balance closure problem: an overview, Ecological Applications, 18, 1351-1367, 10.1890/06-0922.1, 2008.
- García, M., Sandholt, I., Ceccato, P., Ridler, M., Mougin, E., Kergoat, L., Morillas, L., Timouk, F., Fensholt, R., and Domingo, F.: Actual  
 evapotranspiration in drylands derived from in-situ and satellite data: Assessing biophysical constraints, Remote Sensing of  
 Environment, 131, 103-118, 10.1016/j.rse.2012.12.016, 2013.
- Gentine, P., Entekhabi, D., Chehbouni, A., Boulet, G., and Duchemin, B.: Analysis of evaporative fraction diurnal behaviour, Agricultural  
 and Forest Meteorology, 143, 13-29, 10.1016/j.agrformet.2006.11.002, 2007.
- 385 Gentine, P., Entekhabi, D., and Polcher, J.: The Diurnal Behavior of Evaporative Fraction in the Soil–Vegetation–Atmospheric Boundary  
 Layer Continuum, Journal of Hydrometeorology, 12, 1530-1546, 10.1175/2011jhm1261.1, 2011.
- Hatala, J. A., Detto, M., and Baldocchi, D. D.: Gross ecosystem photosynthesis causes a diurnal pattern in methane emission from rice,  
 Geophysical Research Letters, 39, 1-5, 10.1029/2012GL051303, 2012.



- 390 Hersbach, H., Bell, B., Berrisford, P., Hirahara, S., Horányi, A., Muñoz-Sabater, J., Nicolas, J., Peubey, C., Radu, R., and Schepers, D.: The ERA5 global reanalysis, *Quarterly Journal of the Royal Meteorological Society*, 146, 1999–2049, 2020.
- Hund, S. V., Allen, D. M., Morillas, L., and Johnson, M. S.: Groundwater recharge indicator as tool for decision makers to increase socio-hydrological resilience to seasonal drought, *Journal of Hydrology*, 563, 1119–1134, 10.1016/j.jhydrol.2018.05.069, 2018.
- Iribarne, J. V., and Godson, W. L.: *Atmospheric thermodynamics*, Springer Science & Business Media, 2012.
- 395 Jarvis, P. G., and McNaughton, K. G.: Stomatal control of transpiration: scaling up from leaf to region, in: *Advances in ecological research*, Elsevier, 1–49, 1986.
- Johnson, M. S., Couto, E. G., Pinto Jr, O. B., Milesi, J., Santos Amorim, R. S., Messias, I. A. M., and Biudes, M. S.: Soil CO<sub>2</sub> Dynamics in a Tree Island Soil of the Pantanal: The Role of Soil Water Potential, *PLOS ONE*, 8, e64874, 10.1371/journal.pone.0064874, 2013.
- Jung, M., Koirala, S., Weber, U., Ichii, K., Gans, F., Camps-Valls, G., Papale, D., Schwalm, C., Tramontana, G., and Reichstein, M.: The FLUXCOM ensemble of global land-atmosphere energy fluxes, *Scientific Data*, 6, 74, 10.1038/s41597-019-0076-8, 2019.
- 400 Kleidon, A., and Schymanski, S.: Thermodynamics and optimality of the water budget on land: A review, *Geophysical Research Letters*, 35, 10.1029/2008gl035393, 2008.
- Kleidon, A., Schymanski, S., and Stieglitz, M.: Thermodynamics, Irreversibility, and Optimality in Land Surface Hydrology, in: *Bioclimatology and Natural Hazards*, edited by: Štřelcová, K., Mátyás, C., Kleidon, A., Lapin, M., Matejka, F., Blaženec, M., Škvarenina, J., and Holécý, J., Springer Netherlands, Dordrecht, 107–118, 2009.
- 405 Knauer, J., El-Madany, T. S., Zaehle, S., and Migliavacca, M.: Bigleaf—An R package for the calculation of physical and physiological ecosystem properties from eddy covariance data, *PLOS ONE*, 13, e0201114, 10.1371/journal.pone.0201114, 2018.
- Leuning, R., van Gorsel, E., Massman, W. J., and Isaac, P. R.: Reflections on the surface energy imbalance problem, *Agricultural and Forest Meteorology*, 156, 65–74, 10.1016/j.agrformet.2011.12.002, 2012.
- 410 Lovell-Smith, J. W., Feistel, R., Harvey, A. H., Hellmuth, O., Bell, S. A., Heinonen, M., and Cooper, J. R.: Metrological challenges for measurements of key climatological observables. Part 4: atmospheric relative humidity, *Metrologia*, 53, R40–R59, 10.1088/0026-1394/53/1/r40, 2015.
- Ma, H.-Y., Klein, S. A., Xie, S., Zhang, C., Tang, S., Tang, Q., Morcrette, C. J., Van Weverberg, K., Petch, J., Ahlgrimm, M., Berg, L. K., Cheruy, F., Cole, J., Forbes, R., Gustafson Jr, W. I., Huang, M., Liu, Y., Merryfield, W., Qian, Y., Roehrig, R., and Wang, Y.-C.: CAUSES: On the Role of Surface Energy Budget Errors to the Warm Surface Air Temperature Error Over the Central United States, *Journal of Geophysical Research: Atmospheres*, 123, 2888–2909, 10.1002/2017jd027194, 2018.
- 415 Mallick, K., Jarvis, A. J., Boegh, E., Fisher, J. B., Drewry, D. T., Tu, K. P., Hook, S. J., Hulley, G., Ardö, J., Beringer, J., Arain, A., and Niyogi, D.: A Surface Temperature Initiated Closure (STIC) for surface energy balance fluxes, *Remote Sensing of Environment*, 141, 243–261, 10.1016/j.rse.2013.10.022, 2014.
- 420 Martens, B., Miralles, D. G., Lievens, H., van der Schalie, R., de Jeu, R. A. M., Fernandez-Prieto, D., Beck, H. E., Dorigo, W. A., and Verhoest, N. E. C.: GLEAM v3: satellite-based land evaporation and root-zone soil moisture, *Geoscientific Model Development*, 10, 1903–1925, 10.5194/gmd-10-1903-2017, 2017.
- Massmann, A., Gentine, P., and Lin, C.: When Does Vapor Pressure Deficit Drive or Reduce Evapotranspiration?, *Journal of Advances in Modeling Earth Systems*, 11, 3305–3320, 10.1029/2019ms001790, 2019.
- 425 McColl, K. A., Salvucci, G. D., and Gentine, P.: Surface Flux Equilibrium Theory Explains an Empirical Estimate of Water-Limited Daily Evapotranspiration, *Journal of Advances in Modeling Earth Systems*, 11, 2036–2049, 10.1029/2019ms001685, 2019.
- McColl, K. A.: Practical and Theoretical Benefits of an Alternative to the Penman-Monteith Evapotranspiration Equation, *Water Resources Research*, 56, e2020WR027106, 10.1029/2020wr027106, 2020.
- 430 McColl, K. A., and Rigden, A. J.: Emergent simplicity of continental evapotranspiration, *Geophysical Research Letters*, n/a, e2020GL087101, 10.1029/2020gl087101, 2020.
- McNaughton, K., and Spriggs, T.: An evaluation of the Priestley and Taylor equation and the complementary relationship using results from a mixed-layer model of the convective boundary layer, *IAHS publication*, 177, 89–104, 1989.
- McNaughton, K. G., and Jarvis, P. G.: Predicting effects of vegetation changes on transpiration and evaporation, *Water deficits and plant growth*, 7, 1–47, 1983.
- 435 Monteith, J., and Unsworth, M.: *Principles of environmental physics: plants, animals, and the atmosphere*, Academic Press, 2013.
- Monteith, J. L.: Evaporation and environment, *Symposia of the society for experimental biology*, 1965, 205–234.
- Monteith, J. L.: Evaporation and surface temperature, *Quarterly Journal of the Royal Meteorological Society*, 107, 1–27, 10.1002/qj.49710745102, 1981.
- 440 Moon, M., Li, D., Liao, W., Rigden, A. J., and Friedl, M. A.: Modification of surface energy balance during springtime: The relative importance of biophysical and meteorological changes, *Agricultural and Forest Meteorology*, 284, 107905, 10.1016/j.agrformet.2020.107905, 2020.
- Morillas, L., Hund, S. V., and Johnson, M. S.: Water Use Dynamics in Double Cropping of Rainfed Upland Rice and Irrigated Melons Produced Under Drought-Prone Tropical Conditions, *Water Resources Research*, 0, 10.1029/2018wr023757, 2019.



- Novick, K. A., Ficklin, D. L., Stoy, P. C., Williams, C. A., Bohrer, G., Oishi, A. C., Papuga, S. A., Blanken, P. D., Noormets, A., Sulman,  
445 B. N., Scott, R. L., Wang, L., and Phillips, R. P.: The increasing importance of atmospheric demand for ecosystem water and  
carbon fluxes, *Nat Clim Change*, 6, 1023, 10.1038/nclimate3114, 2016.
- Oki, T., and Kanae, S.: Global hydrological cycles and world water resources, *Science*, 313, 1068-1072, 2006.
- Pastorello, G., Trotta, C., Canfora, E., Chu, H., Christianson, D., Cheah, Y.-W., Poindexter, C., Chen, J., Elbashandy, A., Humphrey, M.,  
450 Isaac, P., Polidori, D., Ribeca, A., van Ingen, C., Zhang, L., Amiro, B., Ammann, C., Arain, M. A., Ardö, J., Arkebauer, T., Arndt,  
S. K., Arriga, N., Aubinet, M., Aurela, M., Baldocchi, D., Barr, A., Beamesderfer, E., Marchesini, L. B., Bergeron, O., Beringer,  
J., Bernhofer, C., Berveiller, D., Billesbach, D., Black, T. A., Blanken, P. D., Bohrer, G., Boike, J., Bolstad, P. V., Bonal, D.,  
Bonnefond, J.-M., Bowling, D. R., Bracho, R., Brodeur, J., Brümmer, C., Buchmann, N., Burban, B., Burns, S. P., Buysse, P.,  
455 Cale, P., Cavagna, M., Cellier, P., Chen, S., Chini, I., Christensen, T. R., Cleverly, J., Collalti, A., Consalvo, C., Cook, B. D.,  
Cook, D., Coursolle, C., Cremonese, E., Curtis, P. S., D'Andrea, E., da Rocha, H., Dai, X., Davis, K. J., De Cinti, B., de Grandcourt,  
A., De Ligne, A., De Oliveira, R. C., Delpierre, N., Desai, A. R., Di Bella, C. M., di Tommasi, P., Dolman, H., Domingo, F., Dong,  
G., Dore, S., Duce, P., Dufrêne, E., Dunn, A., Dušek, J., Eamus, D., Eichelmann, U., ElKhidir, H. A. M., Eugster, W., Ewenz, C.  
M., Ewers, B., Famulari, D., Fares, S., Feigenwinter, I., Feitz, A., Fensholt, R., Filippa, G., Fischer, M., Frank, J., Galvagno, M.,  
Gharun, M., Gianelle, D., Gielen, B., Gioli, B., Gitelson, A., Godek, I., Goeckede, M., Goldstein, A. H., Gough, C. M., Goulden,  
460 M. L., Graf, A., Griebel, A., Gruening, C., Grünwald, T., Hammerle, A., Han, S., Han, X., Hansen, B. U., Hanson, C., Hatakka,  
J., He, Y., Hehn, M., Heinesch, B., Hinko-Najera, N., Hörtnagl, L., Hutley, L., Ibrom, A., Ikawa, H., Jackowicz-Korczynski, M.,  
Janouš, D., Jans, W., Jassal, R., Jiang, S., Kato, T., Khomik, M., Klatt, J., Knohl, A., Knox, S., Kobayashi, H., Koerber, G., Kolle,  
O., Kosugi, Y., Kotani, A., Kowalski, A., Kruijt, B., Kurbatova, J., Kutsch, W. L., Kwon, H., Launiainen, S., Laurila, T., Law, B.,  
Leuning, R., Li, Y., Liddell, M., Limousin, J.-M., Lion, M., Liska, A. J., Lohila, A., López-Ballesteros, A., López-Blanco, E.,  
Loubet, B., Loustau, D., Lucas-Moffat, A., Lüers, J., Ma, S., Macfarlane, C., Magliulo, V., Maier, R., Mammarella, I., Manca, G.,  
465 Marcolla, B., Margolis, H. A., Marras, S., Massman, W., Mastepanov, M., Matamala, R., Matthes, J. H., Mazzenga, F.,  
McCaughy, H., McHugh, I., McMillan, A. M. S., Merbold, L., Meyer, W., Meyers, T., Miller, S. D., Minerbi, S., Moderow, U.,  
Monson, R. K., Montagnani, L., Moore, C. E., Moors, E., Moreaux, V., Moureaux, C., Munger, J. W., Nakai, T., Neirynck, J.,  
Nesic, Z., Nicolini, G., Noormets, A., Northwood, M., Noretto, M., Nouvellon, Y., Novick, K., Oechel, W., Olesen, J. E., Ourcival,  
J.-M., Papuga, S. A., Parmentier, F.-J., Paul-Limoges, E., Pavelka, M., Peichl, M., Pendall, E., Phillips, R. P., Pilegaard, K., Pirk,  
470 N., Posse, G., Powell, T., Prasse, H., Prober, S. M., Rambal, S., Rannik, Ü., Raz-Yaseef, N., Reed, D., de Dios, V. R., Restrepo-  
Coupe, N., Reverter, B. R., Roland, M., Sabbatini, S., Sachs, T., Saleska, S. R., Sánchez-Cañete, E. P., Sanchez-Mejia, Z. M.,  
Schmid, H. P., Schmidt, M., Schneider, K., Schrader, F., Schroder, I., Scott, R. L., Sedláč, P., Serrano-Ortiz, P., Shao, C., Shi, P.,  
Shironya, I., Siebicke, L., Šigut, L., Silberstein, R., Sirca, C., Spano, D., Steinbrecher, R., Stevens, R. M., Sturtevant, C., Suyker,  
A., Tagesson, T., Takanashi, S., Tang, Y., Tapper, N., Thom, J., Tiedemann, F., Tomassucci, M., Tuovinen, J.-P., Urbanski, S.,  
475 Valentini, R., van der Molen, M., van Gorsel, E., van Huissteden, K., Varlagin, A., Verfaillie, J., Vesala, T., Vincke, C., Vitale,  
D., Vygodskaya, N., Walker, J. P., Walter-Shea, E., Wang, H., Weber, R., Westermann, S., Wille, C., Wofsy, S., Wohlfahrt, G.,  
Wolf, S., Woodgate, W., Li, Y., Zampedri, R., Zhang, J., Zhou, G., Zona, D., Agarwal, D., Biraud, S., Torn, M., and Papale, D.:  
The FLUXNET2015 dataset and the ONEFlux processing pipeline for eddy covariance data, *Scientific Data*, 7, 225,  
10.1038/s41597-020-0534-3, 2020.
- 480 Penman, H. L.: Natural evaporation from open water, bare soil and grass, *Proceedings of the Royal Society of London. Series A.  
Mathematical and Physical Sciences*, 193, 120-145, 1948.
- Priestley, C. H. B., and Taylor, R. J.: On the Assessment of Surface Heat Flux and Evaporation Using Large-Scale Parameters, *Monthly  
Weather Review*, 100, 81-92, 10.1175/1520-0493(1972)100<0081:otaosh>2.3.co;2, 1972.
- 485 Ramirez, J. A., Hobbins, M. T., and Brown, T. C.: Observational evidence of the complementary relationship in regional evaporation lends  
strong support for Bouchet's hypothesis, *Geophysical Research Letters*, 32, 10.1029/2005gl023549, 2005.
- Raupach, M. R.: Combination theory and equilibrium evaporation, *Quarterly Journal of the Royal Meteorological Society*, 127, 1149-1181,  
10.1002/qj.49712757402, 2001.
- Rigden, A. J., and Salvucci, G. D.: Evapotranspiration based on equilibrated relative humidity (ETRHEQ): Evaluation over the continental  
U.S., *Water Resources Research*, 51, 2951-2973, 10.1002/2014wr016072, 2015.
- 490 Rigden, A. J., and Salvucci, G. D.: Stomatal response to humidity and CO<sub>2</sub> implicated in recent decline in US evaporation, *Global Change  
Biology*, 23, 1140-1151, 10.1111/gcb.13439, 2017.
- Roesch, A., and Schmidbauer, H.: WaveletComp: Computational Wavelet Analysis, 2014.
- Salvucci, G. D., and Gentile, P.: Emergent relation between surface vapor conductance and relative humidity profiles yields evaporation  
rates from weather data, *Proceedings of the National Academy of Sciences*, 110, 6287-6291, 10.1073/pnas.1215844110, 2013.
- 495 Sherwood, S., and Fu, Q.: A Drier Future?, *Science*, 343, 737-739, 10.1126/science.1247620, 2014.
- Stoy, P. C., Mauder, M., Foken, T., Marcolla, B., Boegh, E., Ibrom, A., Arain, M. A., Arneth, A., Aurela, M., Bernhofer, C., Cescatti, A.,  
Dellwik, E., Duce, P., Gianelle, D., van Gorsel, E., Kiely, G., Knohl, A., Margolis, H., McCaughy, H., Merbold, L., Montagnani,  
L., Papale, D., Reichstein, M., Saunders, M., Serrano-Ortiz, P., Sottocornola, M., Spano, D., Vaccari, F., and Varlagin, A.: A data-



- 500 driven analysis of energy balance closure across FLUXNET research sites: The role of landscape scale heterogeneity, *Agricultural and Forest Meteorology*, 171-172, 137-152, 10.1016/j.agrformet.2012.11.004, 2013.
- Tan, C. S., Black, T. A., and Nnyamah, J. U.: A Simple Diffusion Model of Transpiration Applied to a Thinned Douglas-Fir Stand, *Ecology*, 59, 1221-1229, 10.2307/1938235, 1978.
- Thom, A. S.: Momentum, mass and heat exchange of vegetation, *Quarterly Journal of the Royal Meteorological Society*, 98, 124-134, 10.1002/qj.49709841510, 1972.
- 505 Willett, K., Dunn, R., Thorne, P., Bell, S., De Podesta, M., Parker, D., Jones, P., and Williams Jr, C.: HadISDH land surface multi-variable humidity and temperature record for climate monitoring, *Climate of the Past*, 10, 2014.
- Wilson, K., Goldstein, A., Falge, E., Aubinet, M., Baldocchi, D., Berbigier, P., Bernhofer, C., Ceulemans, R., Dolman, H., Field, C., Grelle, A., Ibrom, A., Law, B. E., Kowalski, A., Meyers, T., Moncrieff, J., Monson, R., Oechel, W., Tenhunen, J., Valentini, R., and Verma, S.: Energy balance closure at FLUXNET sites, *Agricultural and Forest Meteorology*, 113, 223-243, 10.1016/S0168-1923(02)00109-0, 2002.
- 510